Experimental analysis and prediction of antisymmetric wave motion in a tapered anisotropic waveguide

Jochen Moll[a)]
Department of Physics, Goethe University of Frankfurt, Max-von-Laue-Strasse 1, Frankfurt am Main 60438, Germany

Tomasz Wandowski, Pawel Malinowski, Maciej Radzienski, Szymon Opoka, and Wieslaw Ostachowicz
Institute of Fluid-Flow Machinery, Polish Academy of Sciences, Fiszera 14 Street, Gdansk 80-231, Poland

(Received 24 January 2015; revised 11 May 2015; accepted 9 June 2015; published online 15 July 2015)

This paper presents experimental results for wave propagation in an anisotropic multilayered structure with linearly varying cross section. Knowing the dispersion and wave propagation properties in such a structure is of great importance for non-destructive material testing and structural health monitoring applications for accurate damage detection and localization. In the proposed study, the wavefield is generated by a circular piezoelectric wafer active sensor and measured by a scanning laser-Doppler-vibrometer. The measurements are compared with a theoretical group delay estimation and a signal prediction for the antisymmetric wave motion along the non-uniform propagation path. The required dispersion curves are derived from the well-known global matrix method for segments of constant thickness. A multidimensional frequency-wavenumber analysis of linescan data and the full wavefield provides further insight of the adiabatic wave motion because the wavenumber changes along the tapered geometry of the waveguide. In addition, it is demonstrated that a terahertz time-domain system can be used in glass-fiber reinforced plastic structures as a tool to estimate the thickness profile of thin structures by means of time-of-flight measurements. This information is particularly important for guided wave-based diagnostics of structures with unknown thickness. © *2015 Acoustical Society of America*. [http://dx.doi.org/10.1121/1.4922823]

[TK] Pages: 299–306

I. INTRODUCTION

Elastic wave propagation in an anisotropic waveguide with slowly varying cross section is a challenging problem because the dispersion properties of the wave modes not only change with frequency, but also with the structural thickness and the direction of wave propagation. This means that the wavenumber, and hence the phase and group velocity, changes for each wave mode continuously.[1] The propagating wave modes are called adiabatic since they adapt to the varying thickness of the structure.[2] For practical applications in non-destructive material testing (NDT) and structural health monitoring (SHM), a precise understanding of the adiabatic wave propagation is required in order to perform an accurate localization of the scatterer, such as a delamination or impact damage. Examples are given by aerospace structures or the hull structure of a ship where the wall thickness changes locally as a result of the optimization of the stress distribution. Knowledge of adiabatic wave propagation is also important for acoustic emission testing where the position of the acoustic event is estimated by data inversion techniques based on time-of-flight measurements.

The nature of wave propagation in plates with constant thickness has been studied for many years.[3] Moreover, dispersion properties for structures with arbitrary but constant cross section can be determined by the semi-analytical finite element (SAFE) method.[4] However, wave propagation in structures with slowly varying cross section has yet received little attention. Most of the studies are limited to structures with isotropic material properties and provide limited experimental analysis.

Wave propagation in waveguides with varying height has been studied by Pagneux and Maurel on a theoretical basis.[5] This work has recently been extended to acoustic wave propagation in waveguides with varying curvature and cross section.[6] Numerical and experimental results for downslope wave propagation in a free elastic plate with linearly varying thickness has been demonstrated.[7] In addition, mode conversion from Lamb waves to adiabatic wave modes has been observed for an elastic plate with Gaussian section variation.[8]

Furthermore, the wave propagation problem in a bonded composite structure with tapered adhesive layer has been studied theoretically.[9] However, thickness variations in the anisotropic layers were not considered there. A technique for pulse dispersion prediction and dispersion compensation in structures with varying cross section is proposed in Refs. 10 and 11. Recently, Moreau *et al.*[12] estimated the wavenumber of guided modes in waveguides with linearly varying thickness.

To the best of the authors' knowledge, this is the first experimental study on guided wave propagation in a multilayered anisotropic waveguide with varying cross section.

[a)]Electronic mail: moll@physik.uni-frankfurt.de

Here, we consider a tapered glass-fiber reinforced plastic (GFRP) structure with 12 segments of constant thickness. Since the actual thickness is unknown, a terahertz time-domain system (THz-TDS) in reflection mode is used to estimate the thickness profile. A special focus is here on anti-symmetric wave motion that is dominant in the considered frequency-thickness range and that can be easily measured by laser-Doppler vibrometry. The wavefield analysis has two parts:

(1) *Group-delay analysis*: The well-known global matrix method (GMM) is used to compute the dispersion characteristics for each layer of constant thickness. Next, the phase and group velocity characteristics are used for a time-frequency analysis that has been introduced for isotropic waveguides by De Marchi *et al.*[10] We predict the antisymmetric wave motion along the wave propagation path, including thickness variation, and determine the error with respect to an anisotropic plate with the same anisotropic material properties but constant thickness.
(2) *Multidimensional frequency-wavenumber analysis*: We calculate two-dimensional and three-dimensional Fourier transforms for frequency-wavenumber domain analysis. A similar approach for isotropic structures has been presented in Ref. 13. In analogy to the short time Fourier transform, we propose a short space Fourier transform to resolve the spatially varying wavenumber distribution along the non-uniform propagation path.

The remainder of the paper is organized in the following way: Section II presents the theoretical background of this paper, including the extraction of dispersion curves in isotropic and anisotropic multilayered waveguides, group delay estimation, and the prediction of wave motion in a plate with linearly varying cross section. Section III describes the laser-Doppler-vibrometry and the THz-TDS setup. Here, results for group delay estimation and signal prediction of adiabatic wave motion are shown along with time-domain and frequency-wavenumber domain analysis of linescan data and full wavefield data. Finally, conclusions are drawn in Sec. IV.

II. THEORETICAL BACKGROUND

A. Dispersion curves in isotropic and anisotropic waveguides

Dispersion curves for Lamb waves propagating in an isotropic structure with constant thickness can be determined by the solution of the well-known Rayleigh-Lamb equation.[14] The result is a dispersion diagram that relates the phase (or group) velocity to the product of frequency and plate thickness. The knowledge of the dispersion properties is important for damage localization procedures, relating the waves time-of-flight to the path that the wave has traveled in the medium.[15] Matrix techniques such as the transfer matrix method (TMM) or GMM[3] can be applied for calculating dispersion curves in multilayered structures. Since the TMM leads to instabilities at large products of frequency and thickness, a generally more stable approach is given by modal solutions of the GMM. An alternative way to determine the dispersion properties of guided waves in waveguides with irregular cross section is given by SAFE techniques.[16] In this paper, we follow the GMM approach for extracting the dispersion curves in the anisotropic multilayered waveguide exploiting third-order plate theory.[17]

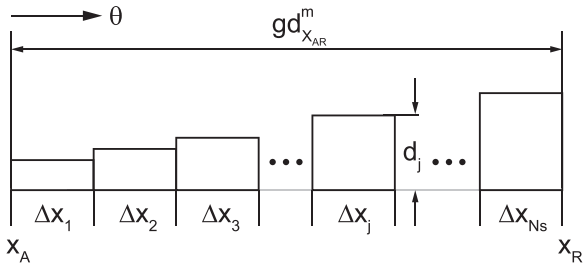

FIG. 1. Schematic of an anisotropic waveguide with varying cross section, where the mth wave mode travels in the θ-direction from the actuator position, x_A, to the receiver position, x_R.

B. Group delay prediction

The group delay, $gd(f,x_R,\theta)$ is a time-frequency approach that determines the time delay for each frequency component, f, at the sensor location, x_R. In contrast to the original formulation,[10] the direction of wave propagation, θ, must be taken into account in anisotropic waveguides. Let us consider a guided wave mode that propagates a distance of $x_{AR} = x_R - x_A$ from the actuator position, x_A, to the location of the receiver, x_R. The propagation path depicted in Fig. 1 covers N_S segments where the jth segment has a length of Δx_j and thickness of d_j. The group delay predictor for the mth guided wave mode is hence defined as

$$gd^m_{x_{AR}}(f,x_R,\theta) = \sum_{j=1}^{N_S} gd^m_j(f,\Delta x_j,\theta) \tag{1}$$

$$= \sum_{j=1}^{N_S} \frac{\Delta x_j}{c^m_{g,j}(f,d_j,\theta)}. \tag{2}$$

This representation accumulates the time delay for each segment, Δx_j, of the waveguide.

C. Prediction of antisymmetric wave motion in a plate with linearly varying cross section

Since the experimental work is based on a tapered GFRP structure, shown later in Fig. 5, the same structure will be considered here first by means of simulation results. The waveguide consists of 12 segments of variable thickness ranging from 0.70 mm to 4.13 mm. The material properties are listed in Table I. A point source is placed at the position $x_A = 0$ mm and a receiver measures the response at $x_R = 600$ mm. The excitation signal is a Hann-modulated tone burst with 1/2 cycles at a carrier frequency of 50 kHz.

TABLE I. Material properties of the GFRP material.

ρ [kg/m^3]	E_{11} [GPa]	E_{22} [GPa]	E_{33} [GPa]	G_{12} [GPa]	G_{13} [GPa]	G_{23} [GPa]	ν_{12}	ν_{13}	ν_{23}
1700	30.7	15.2	10.0	4	3.1	2.75	0.3	0.3	0.3

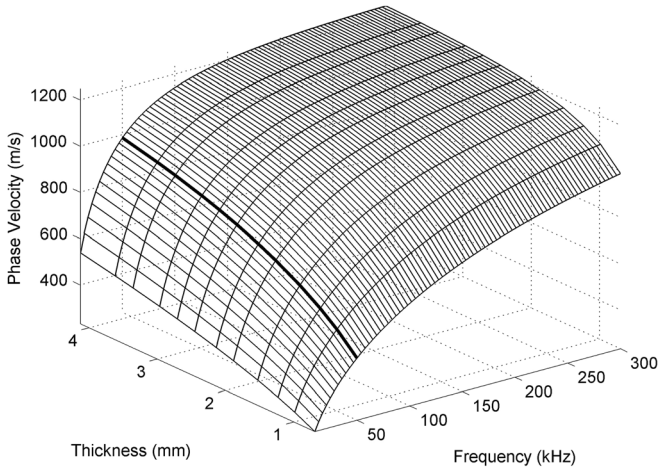

FIG. 2. Phase velocity surface for the fundamental antisymmetric wave mode ($\theta = 90°$). The carrier frequency of 50 kHz is highlighted.

Before presenting the simulation results, Fig. 2 shows the phase velocity and Fig. 3 shows the group velocity surfaces where the carrier frequency of the excitation pulse is highlighted. It can be observed that the velocity increases in a nonlinear way as soon as the structural thickness becomes larger. The frequency of 50 kHz is selected here because this frequency is a compromise between a significant change in velocity due to the varying cross section and the required temporal resolution of the ultrasound waveforms for proper acoustic wavefield imaging in order to discriminate the incident waveform from the echoes reflected from the boundaries of the panel.

For the simulation of wave propagation, we exploit a classical Fourier domain propagation model where we do not account for (i) the radiation pattern of the piezoelectric wafer active sensors (PWASs)[18] and (ii) the mode-selective tuning behavior.[19] Modeling the frequency-dependent excitation of guided waves in generally anisotropic multilayered media is currently under investigation.[20,21] The response at the receiver can be expressed as

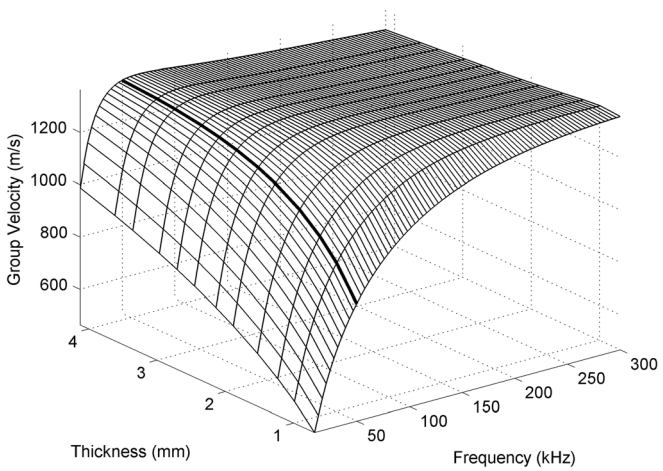

FIG. 3. Group velocity surface for the fundamental antisymmetric wave mode ($\theta = 90°$). The carrier frequency of 50 kHz is highlighted.

$$Y(x_{R,\omega}) = \sum_{j=1}^{N_S} U_e(\omega) \exp(ik_j(\omega,\theta)\Delta x_j). \quad (3)$$

Here, $U_e(\omega)$ denotes the spectrum of the excitation signal and $k_j(\omega,\theta)$ is the frequency-dependent wavenumber of the jth segment in the propagation direction, θ. This term is the solution of the GMM and needs to be computed for each corresponding thickness, d_j; see Fig. 1.

Figure 4(a) illustrates the dispersive response of the fundamental antisymmetric wave mode at the (virtual) PWAS receiver position, x_R. The corresponding time frequency representation in Fig. 4(b) is based on the reassigned spectrogram and further includes the group delay estimation. It can be observed that the group delay prediction matches exactly the simulated signal, showing that the group delay concept can be applied successfully to anisotropic waveguides with varying thickness assuming that no wave mode conversion occurs. For the two limiting values of thickness of the investigated panel, namely, 0.7 mm and 4.13 mm, the group delay curves for a constant thickness plate composed of the same material are plotted in the same figure. As soon as a plate with constant thickness is assumed, significant deviations from the theoretical group delay prediction occur, which would cause severe damage localization errors in NDT and SHM applications.

III. RESULTS

A. Experimental setup for acoustic wavefield measurements

Figure 5 shows a schematic of the experimental setup used in this work. A circular surface-bonded PWAS with a diameter of 10 mm is glued exactly in the middle of the structure at (0.25 m, 0.30 m) and generates adiabatic wave modes. The PWAS is made by CeramTec Company (Lauf, Germany) and consists of Sonox P502 material with a thickness of 0.5 mm. One of the silver electrodes is wrapped

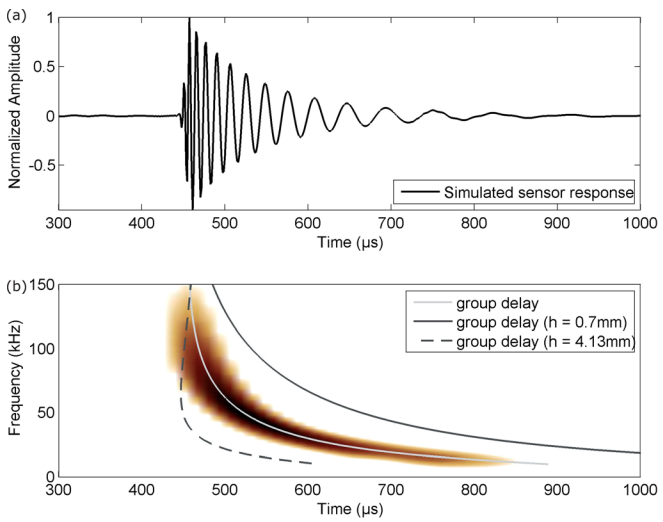

FIG. 4. (Color online) (a) Dispersive sensor response at the receiver location, $x_R = 600$ mm. (b) Reassigned spectrogram and corresponding group delay predictions.

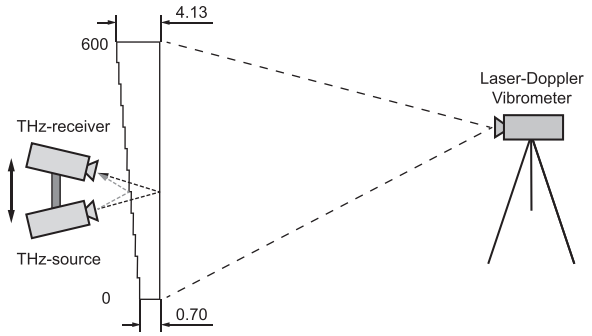

FIG. 5. Measurement setup for the structure with 12 segments of constant thickness: THz-TDS for thickness estimation and laser-Doppler-vibrometer for acoustic wavefield measurement.

around allowing for wires soldering on one face of the sensors. The signal for the PWAS is provided by the TTi TG4001 arbitrary function generator (Huntingdon, Cambridgeshire, UK) and is later amplified up to 200 V in order to ensure high signal-to-noise ratio.

While the actuating PWAS is placed on the segmented surface of the sample, the wave sensing is realized on the flat surface (Fig. 5). The wave registration is achieved with a non-contact device—a scanning laser-Doppler-vibrometer (SLDV). In order to achieve a good reflectivity for the laser measurements, the surface is covered with retroreflective adhesive tape that reflects the laser light back to the vibrometer head (Fig. 6). A SLDV measures the out-of-plane components of the wavefield excited by the PWAS. In our research, the Polytec® PSV 400 SLDV (Waldbronn, Germany) is used. In the considered frequency range, the out-of-plane vibration is mostly related to the antisymmetric wave motion. The wavefield excited by the PWAS and registered by the SLDV is depicted in Fig. 7. A distortion of the wavefield in the horizontal direction can be observed in the snapshot at 254 μs due to the anisotropic character of the GFRP material. The changing propagation velocity can be seen in the vertical direction since the waveform arrives at the top edge prior to the bottom edge.

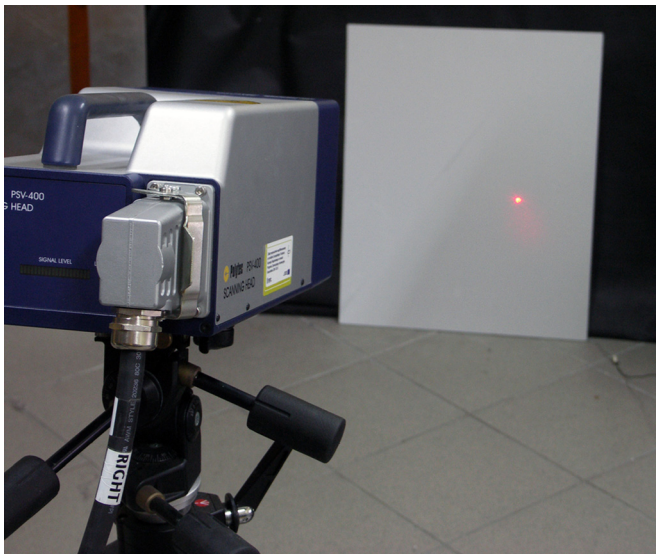

FIG. 6. (Color online) Experimental setup for measuring the out-of-plane motion of guided waves by a SLDV.

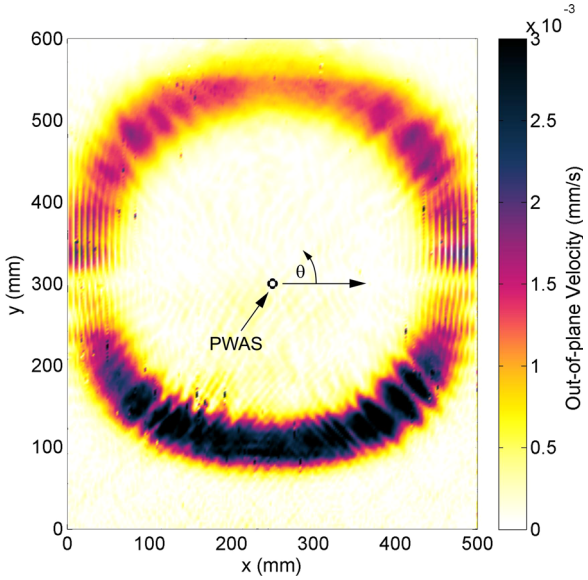

FIG. 7. (Color online) The actuating PWAS is placed in the center of the structure at (0.25 m, 0.30 m). The snapshot at 254 μs shows a distortion of the wavefield in the horizontal direction due to the anisotropic character of the GFRP material. In the vertical direction, the changing propagation velocity can be observed since the waveform arrives at the top edge prior to the bottom edge.

B. Thickness estimation by terahertz time-domain analysis

Terahertz time-domain spectroscopy (TDS) in the frequency range from 100 GHz to ~4 THz has been used in recent years for the purpose of NDT.[22] The submillimeter-waves are able to penetrate through many nonconducting materials. At each dielectric interface, e.g., from air to the GFRP- material, the electromagnetic waves experience partial transmission and reflection. In this paper, we use the THz-TDS system as a tool to remotely measure the thickness of the composite structure; compare Refs. 23 and 24. The scanning heads of the THz-TDS system have been working in reflection mode, which means that the source of radiation and receiver are both on the same side of the sample (Fig. 8). THz-TDS system TPS Spectra 3000+ by TeraView Limited

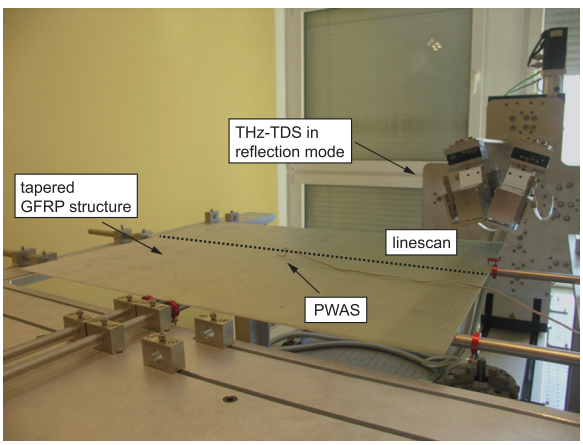

FIG. 8. (Color online) THz-TDS system with scanning heads working in reflection mode to measure the thickness of the tapered GFRP structure. The linescan is performed in the direct vicinity of the PWAS.

(Cambridge, UK) generates radiation in the form of repeated, very narrow picosecond pulses, which are focused and sent toward the investigated structure. Wide frequency content, small power, and non-ionizing radiation are the main characteristics of the pulse.

This approach is very interesting when the material is transparent at THz frequencies, such as GFRP, and the geometry of the structure is unknown. Then, a single side access can be used to precisely measure the thickness, which is important information for guided wave analysis for composite panels with glass fibers. The experimental setup using the THz-TDS system is shown in Fig. 8 where the investigated panel is supported by several steel bars that belong to the THz system. The whole part is moved in the horizontal direction to record the linescan measurements. Above the panel, the scanning heads are located where the distance between the heads and panel is restricted by the external optics of the system. Figure 9(a) shows the raw terahertz linescan signals in the form of a B-scan that has been low-pass filtered using a Butterworth filter with a cutoff frequency of 1.7 THz and a filter order of $N_f = 4$. This reduces, as shown in Fig. 9(b), the measurement noise and optimizes the accuracy for the thickness measurement. A direct comparison of the terahertz waveforms at the location $y = 200\,\text{mm}$ is shown in Fig. 9(c). Based on simple time-of-flight signal processing, the local maxima of the waveforms can be extracted.

Assuming a relative permittivity of $\varepsilon_{r,\text{GFRP}} = 1.7$, the thickness of the ith segment can be determined by

$$t_i = 0.5\frac{c_0 \Delta T}{\sqrt{\varepsilon_{r,GFRP}}}. \tag{4}$$

Here, c_0 denotes the speed of light in vacuum and ΔT is the time difference between the local maxima of the THz waveforms, i.e., front- and back-wall reflection. The factor 0.5 accounts for the round-trip time due to the reflection setup (propagation from the source, reflection, and back propagation to the receiver; Fig. 8). A good agreement between the caliper measurements (at the edge of the panel) and the THz-based estimation (linescan measurement in the middle of the structure) can be observed in Fig. 9(d). Certain bending effects of the sample caused by gravity cannot be avoided in the horizontal setup, but the proposed time-of-flight-procedure is able to correct for this mechanical deformation automatically.

C. Prediction of antisymmetric wave motion in a tapered anisotropic waveguide

The thickness profile extracted from the THz measurements in Sec. III B is now the input for the GMM and the prediction of the receiver signal. Again, the material model from Table I is selected. Figure 10(a) illustrates the vertical linescan signals that are taken from the full wavefield at the horizontal position of the PWAS at $x = 250\,\text{mm}$. Although the PWAS is located in the center of the structure, the antisymmetric waveform arrives much faster at the thicker end of the structure at $y = 600\,\text{mm}$ due to the higher propagation velocity in that direction. Conversely, a longer propagation time can be observed when the antisymmetric waveform travels to the thinner end of the structure at $y = 0\,\text{mm}$. The reason, therefore, is a reduced wave velocity that can be observed in Fig. 3.

The requirement for the signal prediction is to account for these variations in wave velocity. Thus, two equidistant measurement points having both a distance to the PWAS of 250 mm are taken as examples. The results are shown in Figs. 10(b) and 10(c). In both cases a good agreement was

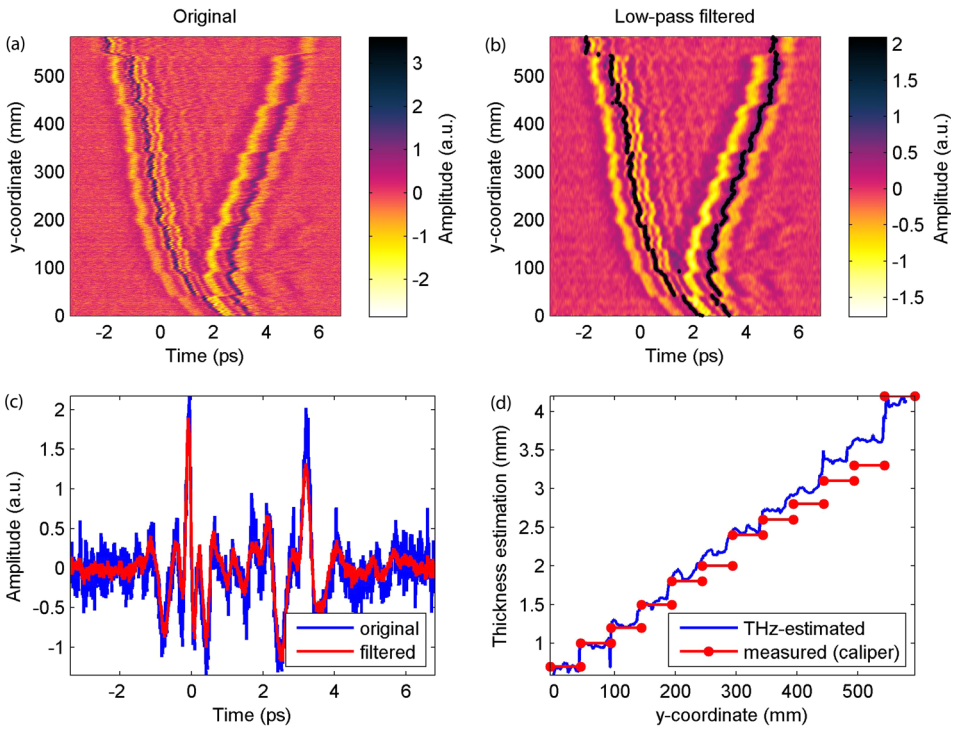

FIG. 9. (Color online) (a),(b) Terahertz B-scan of the original and the low-pass filtered THz-waveforms. (c) Comparison of terahertz waveforms before and after low-pass filtering. (d) Thickness estimation based on time-of-flight analysis in Eq. (4). The reference measurements have been taken with a caliper at the edge of the panel; the THz waveforms are recorded in the middle of the panel close to the PWAS.

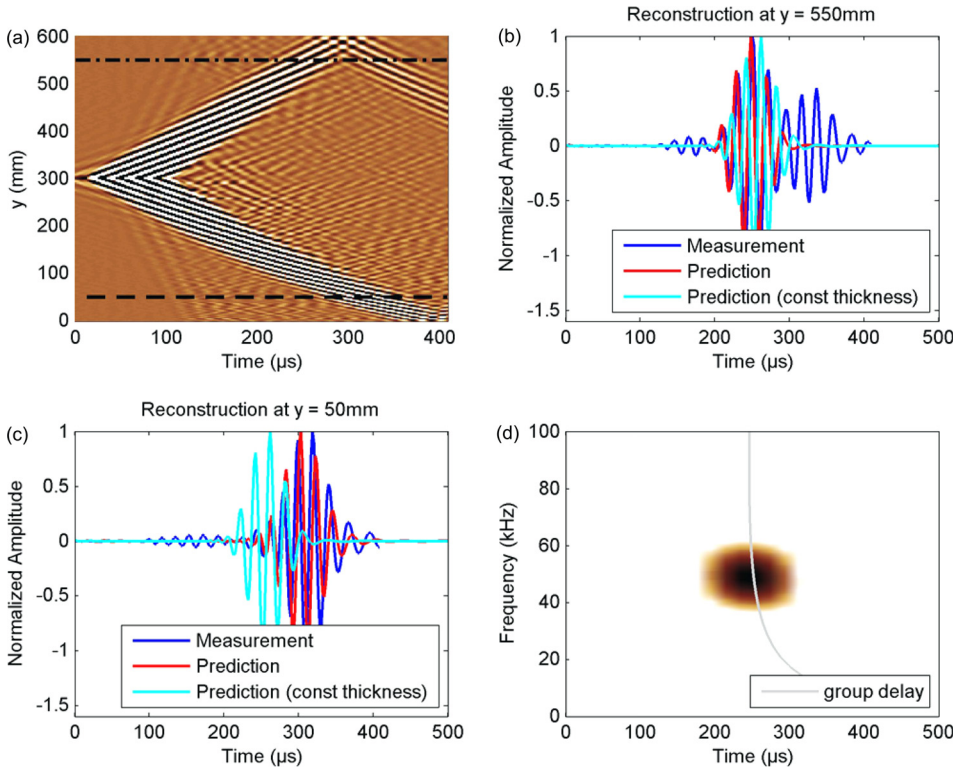

FIG. 10. (Color online) (a) Vertical linescan data at the location of the PWAS. (b) Measurement and signal prediction at $y = 550$ mm. (c) Measurement and signal prediction at $y = 50$ mm. (d) Reassigned spectrogram and group delay curve at $y = 550$ mm.

found between the measured and the predicted signals, although the arrival times in both cases are significantly different. Small deviations in phase are due to uncertainties in the THz-based thickness estimation as shown in Fig. 9(d), which is the input for the theoretical dispersion properties. In order to evaluate the error with respect to a structure of uniform thickness, the dispersion properties of the antisymmetric wave mode at the location of the PWAS is considered. This is a reasonable assumption since the PWAS is located at the medium thickness of the tapered structure. Figure 10(b) shows a relatively small error of 11.7 μs between the measurement and the prediction for the uniform thickness. This can be explained by Fig. 3 because the group velocity does not change much toward greater structural thickness. However, a large time delay of 56.7 μs occurs at the measurement position $y = 50$ mm in Fig. 10(c). Here, the changes in group velocity become more significant. It can be concluded that the signal prediction works fine when the tapered geometry of the structure is taken into account. Otherwise, a significant error in time delay occurs that cannot be neglected in NDT and SHM applications.

Furthermore, Fig. 10(d) depicts the reassigned spectrogram of the signal in Fig. 10(b) supported by the estimated group delay. Since a narrowband excitation signal is used in the experiment, the shape of the time-frequency representation is substantially different compared to Fig. 4. However, a good agreement can be observed between the measured signal and the group delay prediction.

D. Multidimensional Fourier-domain analysis

1. Vertical line of points analysis

From the full wavefield data registered with the SLDV, a vertical line of 249 points crossing the center of the specimen was chosen for frequency-wavenumber analysis. Two excitation scenarios were considered: Hanning windowed sinusoidal bursts with three cycles at carrier frequencies of 50 kHz and 100 kHz.

In order to transform the signal from time-space domain (t-y) to frequency-wavenumber space (f-k_y-y) domain two-dimensional short space Fourier Transform (2D-SSFT) may be used as

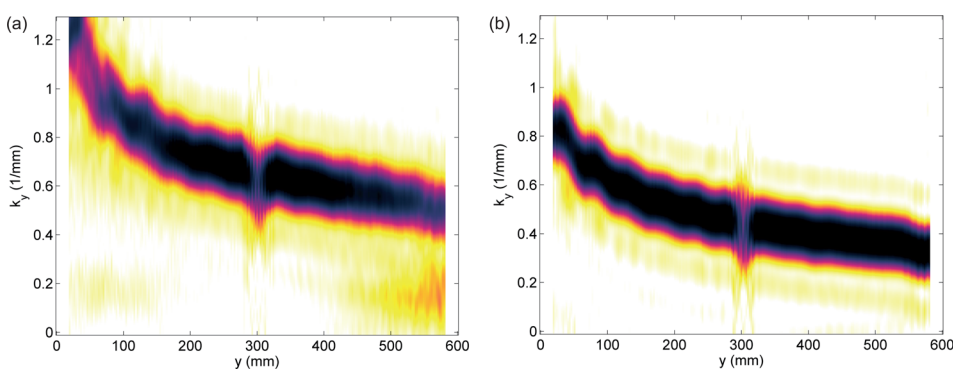

FIG. 11. (Color online) Wavenumber-space domain (k_y-y) for burst excitation at a central frequency of (a) 50 kHz and (b) 100 kHz.

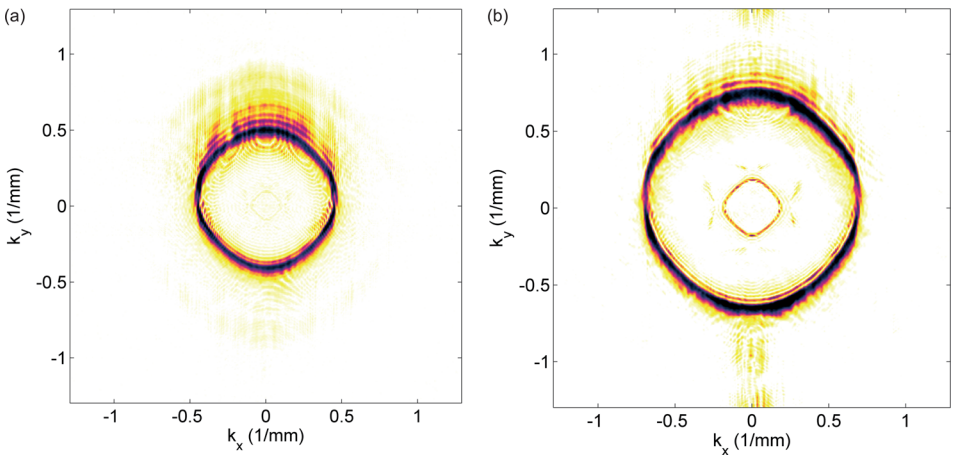

FIG. 12. (Color online) Wavenumber-frequency domain (k_x-k_y-f) at central frequency for burst excitation with a central frequency of (a) 50 kHz and (b) 100 kHz.

$$V(f,k_y,\alpha)=\int_{-\infty}^{\infty}\int_{-\infty}^{\infty}v(t,y)W(y-\alpha)e^{-j(2\pi ft-k_y y)}dtdy, \tag{5}$$

where $W(y)$ denotes the window function and α stands for the translation of the window function, $W(y)$, along y-dimension. This enables the analysis of a spatially varying wavenumber pattern along the non-uniform propagation path. To visualize the data, integration over the considered frequency range (F) of the signal may be used

$$\bar{V}(k_y,\alpha)=\int_F V(f,k_y,\alpha). \tag{6}$$

It should be noted that increasing the width of the window function, $W(y)$, will increase the resolution in wavenumber, but decreases the resolution in space domain at the same time. The result of processing the 2D-SSFT is visualized in Fig. 11. It can be observed that the wavenumber as a function of y-dimension decreases when the specimens thickness increases.

2. Full wavefield analysis

With the purpose of transforming full wavefield data from time-space domain (t-x-y) to frequency-wavenumber-domain (f-k_x-k_y) a three-dimensional Fourier transform (3D FT) may be used as

$$V(f,k_y)=\int_{-\infty}^{\infty}\int_{-\infty}^{\infty}\int_{-\infty}^{\infty}v(t,x,y)e^{-j(2\pi ft-k_x x-k_y y)}dtdxdy. \tag{7}$$

Two images were created based on the 3D FT and presented at the carrier frequency of the excitation pulse, i.e., 50 kHz and 100 kHz, in Fig. 12. It can be observed that

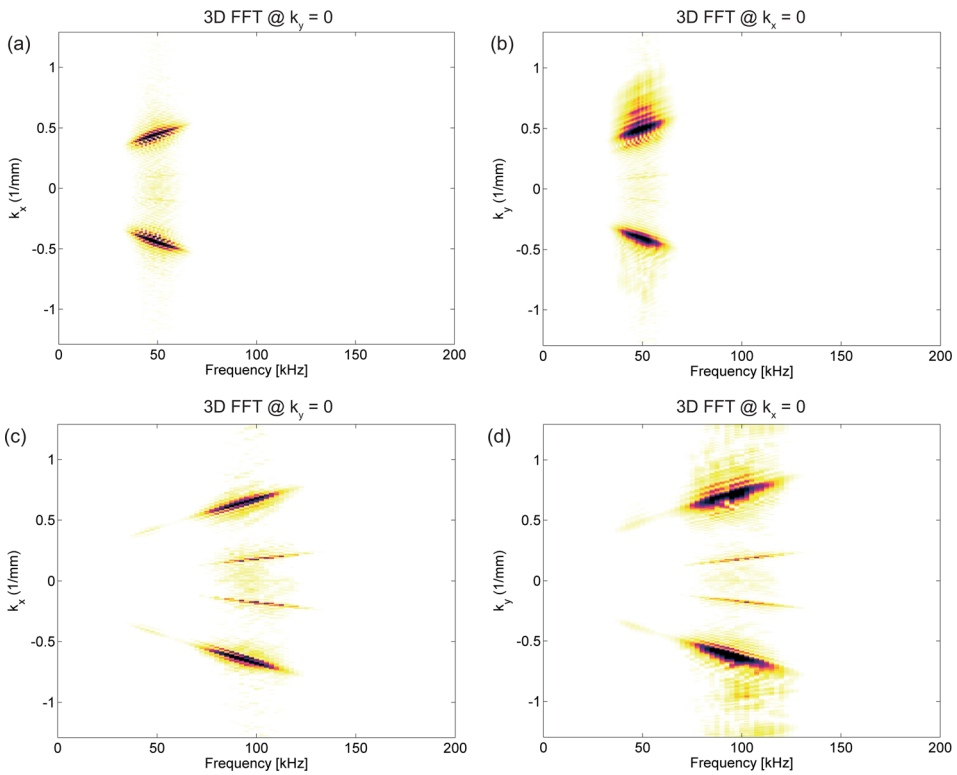

FIG. 13. (Color online) Slice of the 3D-Fourier transform for the carrier frequencies (a),(b) 50 kHz and (c),(d) 100 kHz.

changes in wavenumber, k_y, creates multiple parallel lines in this direction. This phenomenon does not occur in the k_x-direction due to constant thickness of the specimen in the x-direction.

Further information about the wavefield can be obtained by the k_x-f-representation ($k_y = 0$) shown in Figs. 13(a) and 13(c) and the k_y-f-representation ($k_x = 0$) shown in Figs. 13(b) and 13(d) for the two carrier frequencies of interest. It can be observed for both cases that the blurring in the k_x-direction is almost zero given the fact that the structure has a constant thickness in that direction. On the contrary, a significant blurring can be observed in the k_y-direction due to the changing wavelength. Although the focus of this paper is on the analysis of the antisymmetric wave mode, the symmetric wave mode can be clearly identified in Figs. 13(c) and 13(d). The mode tuning-effect of the piezoelectric transducers, discussed e.g., in Ref. 19, is responsible for the fact that the symmetric wave mode can be observed at 100 kHz and cannot be observed at 50 kHz.

IV. CONCLUDING REMARKS

The novelty of this paper is to study the wave propagation of the antisymmetric wave motion in a tapered anisotropic waveguide through theoretical and experimental investigations. Besides the well-known measurement procedure of scanning laser-Doppler vibrometry, we demonstrated the performance of terahertz time-domain analysis in reflection mode to extract the thickness information of the GFRP structure. It was shown that the phase and group velocity of the antisymmetric wave mode changes strongly when the thickness of the structure increases. This observation is important for many practical applications in the context of NDT and SHM. Moreover, a good agreement was found between the theoretical prediction of the receiver response and the measured signals. As soon as the non-uniform geometry of the structure is neglected, a significant error in the time of arrival occurred. Analyzing the full wavefield in the frequency-wavenumber domain revealed a significant blurring due to the spatially varying wavenumber characteristic.

Animations presenting several results from the multi-dimensional Fourier transforms at the whole frequency range may be found attached to the online version of this paper as supplemental material.[25]

ACKNOWLEDGMENTS

This work was supported by Grant No. PBS1/B6/8/2012 (project KOMPNDT) of the Polish National Centre for Research and Development (NCBR). The authors are grateful for the financial support provided by the National Science Centre of Poland granted by decision number DEC-2012/06/M/ST8/00414. Moreover, the authors would like to thank Dr. Miguel Angel Torres Arredondo (MAN Diesel & Turbo, Augsburg, Germany) for discussions about the calculation of dispersion curves in anisotropic multilayered composite materials and Dr. Luca De Marchi (University of Bologna) for discussions on group delay computation.

[1]V. B. Galanenko, "On coupled modes theory of two-dimensional wave motion in elastic waveguides with slowly varying parameters in curvilinear orthogonal coordinates," J. Acoust. Soc. Am. **103**, 1752–1762 (1998).
[2]J. M. Arnold and L. B. Felsen, "Coupled mode theory of intrinsic modes in a wedge," J. Acoust. Soc. Am. **79**, 31–40 (1986).
[3]M. Lowe, "Matrix techniques for modeling ultrasonic waves in multilayered media," IEEE Trans. Ultrason., Ferroelectr. Freq. Control **42**, 525–542 (1995).
[4]P. Bocchini, A. Marzani, and E. Viola, "Graphical user interface for guided acoustic waves," J. Comput. Civ. Eng. **25**, 202–210 (2011).
[5]V. Pagneux and A. Maurel, "Lamb wave propagation in elastic waveguides with variable thickness," Proc. R. Soc. London, Ser. A **462**, 1315–1339 (2006).
[6]A. Maurel, J.-F. Mercier, and S. Felix, "Propagation in waveguides with varying cross section and curvature: A new light on the role of supplementary modes in multi-modal methods," Proc. R. Soc. London, Ser. A **470**, 20140008 (2014).
[7]M.-C. El-Kettani, F. Lupp, and A. Guillet, "Guided waves in a plate with linearly varying thickness: Experimental and numerical results," Ultrasonics **42**, 807–812 (2004).
[8]P. Marical, M. Ech-Cherif El-Kettani, and M. Predoi, "Guided waves in elastic plates with Gaussian section variation: Experimental and numerical results," Ultrasonics **47**, 1–9 (2007).
[9]Q.-T. Deng and Z.-C. Yang, "Propagation of guided waves in bonded composite structures with tapered adhesive layer," Appl. Math. Modell. **35**, 5369–5381 (2011).
[10]L. De Marchi, A. Marzani, N. Speciale, and E. Viola, "Prediction of pulse dispersion in tapered waveguides," NDT&E Int. **43**, 265–271 (2010).
[11]L. De Marchi, A. Marzani, and M. Miniaci, "A dispersion compensation procedure to extend pulse-echo defects location to irregular waveguides," NDT&E Int. **54**, 115–122 (2013).
[12]L. Moreau, J.-G. Minonzio, M. Talmant, and P. Laugier, "Measuring the wavenumber of guided modes in waveguides with linearly varying thickness," J. Acoust. Soc. Am. **135**, 2614–2624 (2014).
[13]Z. Tian and L. Yu, "Lamb wave frequency-wavenumber analysis and decomposition," J. Intell. Mater. Syst. Struct. **25**, 1107–1123 (2014).
[14]J. L. Rose, *Ultrasonic Waves in Solid Media* (Cambridge University Press, Cambridge, New York, 1999), pp. 1–476.
[15]J. Moll, R. Schulte, B. Hartmann, C.-P. Fritzen, and O. Nelles, "Multi-site damage localization in anisotropic plate-like structures using an active guided wave structural health monitoring system," Smart Mater. Struct. **19**, 045022 (2010).
[16]Z. Fan, "Applications of guided wave propagation on waveguides with irregular cross-section," Ph.D. thesis, Imperial College London, UK, 2010, pp. 1–172.
[17]M. Torres Arredondo, M. Ramirez Lozano, and C.-P. Fritzen, "DispWare toolbox—A scientific computer program for the calculation of dispersion relations for modal-based acoustic emission and ultrasonic testing," Technical Report, University of Siegen, Germany (2011), pp. 1–177.
[18]J. Moll, M. Golub, E. Glushkov, N. Glushkova, and C.-P. Fritzen, "Non-axisymmetric Lamb wave excitation by piezoelectric wafer active sensors," Sens. Actuators, A **174**, 173–180 (2012).
[19]V. Giurgiutiu, "Tuned Lamb wave excitation and detection with piezoelectric wafer active sensors for structural health monitoring," J. Intell. Mater. Syst. Struct. **16**, 291–305 (2005).
[20]E. Glushkov, N. Glushkova, A. Eremin, R. Lammering, and M. Neumann, "Frequency dependent directivity of guided waves excited by circular transducers in anisotropic composite plates," J. Acoust. Soc. Am. **132**, EL119–EL124 (2012).
[21]A. Velichko and P. D. Wilcox, "Modeling the excitation of guided waves in generally anisotropic multilayered media," J. Acoust. Soc. Am. **121**, 60–69 (2007).
[22]C. Stoik, M. Bohn, and J. Blackshire, "Nondestructive evaluation of aircraft composites using reflective terahertz time domain spectroscopy," NDT&E Int. **43**, 106–115 (2010).
[23]T. D. Dorney, R. G. Baraniuk, and D. M. Mittleman, "Material parameter estimation with terahertz time-domain spectroscopy," J. Opt. Soc. Am. A **18**, 1562–1571 (2001).
[24]L. Duvillaret, F. Garet, and J.-L. Coutaz, "Highly precise determination of optical constants and sample thickness in terahertz time-domain spectroscopy," Appl. Opt. **38**, 409–415 (1999).
[25]See supplementary material at http://dx.doi.org/10.1121/1.4922823 for a wave-field animation at a carrier frequency of 50 kHz and 100 kHz, respectively, as well as animated slices through the multidimensional Fourier transform for both datasets, i.e., 50 kHz and 100 kHz.